Materials Chemistry Horizons RESEARCH

Synthesis of Poly(*N*-vinylpyrrolidone)-*grafted*-magnetite bromoacetylated cellulose via ATRP for Drug Delivery

Nasim Movagharnezhad, Sedigheh Ehsanimehr, Peyman Najafi Moghadam*

Department of Applied Chemistry, Faculty of Chemistry, Urmia University, Urmia 57153-165, Iran

Corresponding author: p_najafi27@yahoo.com (P. Najafi Moghadam)

Mater. Chem. Horizons, 2022, 1(2), 89-98 10.22128/mch.2022.545.1004 OPEN ACCESS

ABSTRACT

In the present article, we have reported a detailed study of the surface modification for magnetite nanoparticles (MNP, Fe_3O_4) using a natural, biodegradable, and biocompatible polymer. For this purpose, the cellulose was converted to its bromoacetylated derivative (BACell) by reacting with bromoacetyl bromide. Next, the MNPs were functionalized by the reaction of the hydroxyl groups with the methylene bromide of the prepared BACell to form Fe_3O_4/BACell. Then, the atom transfer radical polymerization (ATRP) method was developed for the covalent immobilization of the *N*-vinylpyrrolidone (NVP) on the Fe_3O_4/BACell surface to produce the Fe_3O_4/Cellulose-grafted NVP (Fe_3O_4/Cell-NVP) as a novel synthetic product. The Fourier transform infrared spectroscopy (FT-IR) indicated the presence of copolymer on the MNPs surface. Moreover, the thermogravimetric analysis (TGA) results of the Fe_3O_4/Cell-NVP indicated that there had been an acceptable percentage of the content of polymer chains on the surface of the Fe_3O_4 nanoparticles. Furthermore, the structure and magnetic properties of the Fe_3O_4/Cell-NVP were confirmed by X-ray diffraction (XRD), vibrating sample magnetometer (VSM), and scanning electron microscopy (SEM). The loading capacity and release profiles of Doxorubicin (DOX) as a model drug from the Fe_3O_4/Cell-NVP were determined by UV–Vis absorption measurement at λ_{max}=483 nm. The results showed that the DOX-loaded nanoparticles had been well controlled during the release period of the DOX. Therefore, it seems that the Fe_3O_4/Cell-NVP is an appropriate candidate for the controlled and targeted delivery of cancer treatment.

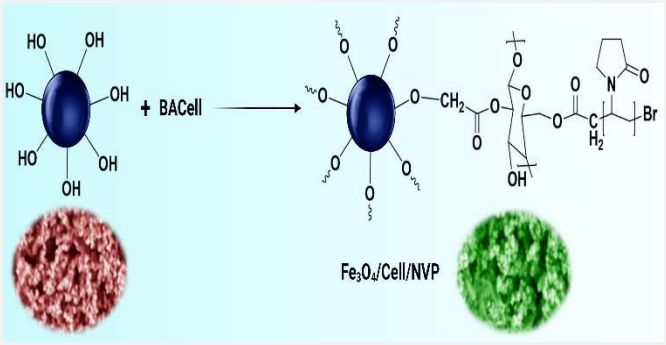

Keywords: Magnetic nanoparticles, cellulose, ATRP, doxorubicin, controlled drug delivery

1. Introduction

In recent years, there has been an increased interest in using nanotechnology. Thus, some different uses of newly developed nanomaterials have been investigated. Nanotechnology has attracted more attention due to demonstrated improvements in electronic, optical, magnetic, mechanical, and thermal properties [1-5]. Among the various nanoparticle types, the Magnetite nanoparticles (MNPs) are widely studied because they have superparamagnetism which means they can redisperse when the external magnetic field withdraws. Therefore, the MNPs generate excellent materials in biomedical applications such as magnetic resonance imaging (MRI), contrast enhancement, drug delivery, tissue repair, cell labeling, and magnetic cell sorting [6-13].

However, the MNPs which have a reactive surface must be coated with a stable shell and a biocompatible material to avoid its potential toxic effects on the cells [14]. Consequently, suitable protection strategies of the MNPs are very necessary for most of their applications [15]. Several methods have been developed to prepare a polymeric shell on the MNPs including physical adsorption of polymers, emulsion polymerization in the presence of the MNPs, and a "grafting to" method [16-17].

Received: May 22, 2022
Received in revised: June 11, 2022
Accepted: July 12, 2022
This is an open access article under the CC BY license.

The "grafting-to" technique is the most attractive one because of its effectiveness to modify the chemical and physical properties of the MNPs. Among the various "grafting-to" methods for polymer attachment, surface-initiated atom-transfer radical polymerization (ATRP) is an excellent technique to synthesize well-defined nanostructures [18, 19]. In an ATRP method, a metal that is complexed by an appropriate ligand is used to transfer a halogen atom from the initiator to the monomer [20].

Various materials have been used for the "grafting-to" MNPs such as polystyrene [21], poly (vinyl alcohol) [22], poly (glycidyl methacrylate) [23], dextran [24], and cellulose. Among them, cellulose receives great attention as a potential material to produce advanced materials. The cellulose which is the most abundant, biodegradable, and biocompatible component of the non-food biomass is a water-insoluble saccharide polymer composed of glucose monomers and linked by ß-1, 4 glycosidic bonds [25-27]. Many efforts have been made to prepare the MNP drug carriers with cellulose derivatives. Fidale et al. [28] demonstrated an efficient strategy to form Fe_3O_4@aminocellulose hybrid nanoparticles. Mallick et al. [29] employed a green, facile, and one-pot wet chemical method to optimize the formulation of the super-paramagnetic iron oxide nanoparticles capped with carboxymethyl cellulose. Elumalai et al. [30] prepared a novel protamine and carboxymethyl cellulose polyelectrolyte multi-layered nanocapsules modified with Fe_3O_4 nanoparticles to deliver the doxorubicin against highly drug-resistant HeLa cells.

Natural cellulose which finds an application in a biomedical field like the drug delivery carriers have been found to possess a wide range of properties [31]. However, cellulose suffers from some disadvantages such as low mechanical strength and poor processability, so modification of the cellulose has been carried out to overcome these limitations. In this study, a bromoacetylated derivative of the cellulose was prepared and used to modify the Fe_3O_4 NPs to form a Fe_3O_4/BACell as an ATRP macroinitiator. Then the copper-mediated ATRP technique was used to graft the polymerization of N- vinylpyrrolidone (NVP) on the Fe_3O_4/BACell surface and the Fe_3O_4/Cell-NVP was produced. The magnification of the modified cellulose developed the controlled drug delivery systems. Characterization was performed using FTIR, XRD, TGA, VSM, and SEM analyses. Quantitative measurements of the loading and releasing processes of doxorubicin (DOX) as a model anticancer drug was carried out using the UV–Vis measurement in two different pHs (bicarbonate buffer solutions: pH=5 and pH=7.4) and they showed a good controlled release of the DOX. The results showed that the Fe_3O_4/Cell-NVP can be used for an appropriate application as the targeted drug delivery.

2. Experimental

2.1. Materials

The cellulose powder (Merck, Germany: 102330) was pulverized, dried in a vacuum for 24h, and kept in a desiccator. The doxorubicin was obtained from Sigma (Sigma, United States: D4035). Bo Cu (1) bromide (CuBr, Aldrich, United States: 212865) was used without further purification. The Bromoacetyl bromide (>99%, 820174)), pyridine (107462), pentamethyl diethylene triamine (PMDETA, 841692), *N*- vinylpyrrolidone (NVP, 808518), N, N-dimethyl acetamide (DMAc, 803235), and dimethyl formamide (DMF, 822275) were obtained from Merck Germany. LiCl (99.95%, Merck, Germany: 105677) was kept under the vacuum oven overnight to remove any trace moisture before use. The iron oxide nanoparticles (Fe_3O_4) were purchased from Us Research Nanomaterials, Inc. (United State: US3208).

2.2. Measurements

The spectra of the FT-IR were measured with a Fourier Transform Infrared spectrophotometer (Nexus 670, Thermo Nicolet, USA). The Thermal Gravimetric Analysis (TGA) of the prepared samples was determined using the LENSESSTAPT-1000 calorimeter (Germany) by Scanning from room temperature up to 650 °C with a heating rate of 10°C/min. The spectra of the XRD were recorded on an X'Pert Proan X-ray photoelectron spectrometer (Netherlands) using the nonmono-chromated Cu Kα radiation as an excitation source. A vibrating sample magnetometer (VSM, Newcastle-upon-Tyne, UK) was used to study the magnetic properties of the MNPs. Moreover, the morphology of the samples was observed by scanning the electron microscopy (SEM) images which were obtained

by using a SEM-3200 scanning electron microscope. Furthermore, the UV-Vis. A spectrophotometer (T80 – PG Instruments Ltd. UK) was used to study the drug release.

2.3. Preparations of bromoacetylated cellulose (BACell)

The DMAc/LiCl (20 mL, 2.5 w/w%) was added into a 50 mL round-bottom flask equipped with a magnetic stirring bar, then the cellulose powder (1 g, 6.17 mmol) was added too. The flask was kept under reflux at 80°C for about 2 hrs. and then it was cooled down to room temperature. After that pyridine (1.46 g, 18.51mmol) and bromoacetyl bromide (4.48 g, 22.22 mmol) were added slowly to the flask with stirring in the ice bath. After the addition was completed, stirring was continued at room temperature for 18 hrs. Finally, the mixture was poured in 150 mL HCl 2 M, and (Placeholder1) was filtered and washed several times with distilled water, and eventually, it was dried under the vacuum oven at 50°C.

2.4. Modification of MNPs with BACell

The magnetite nanoparticle surface was modified by the reaction of the BACell with the hydroxyl groups located on the Fe_3O_4 external surface. In a general procedure, the naked MNPs (100 mg) were put in a one-necked flask which was containing DMA (10 mL), and then it was kept in an ultrasonic bath for 20 min to obtain a homogenous dark solution. After that, required amounts of the BACell (2% w/v) and pyridine (0.3 w/v) were added to the solution and the reaction mixture was again ultrasonicated for 20 min. and then a magnetic stirrer was added to the flask for further reaction time. The reaction mixture was stirred at 60 °C under a nitrogen atmosphere for 24 hrs. The product was recovered from the reaction mixture by a permanent magnet and then it was washed with methanol several times to produce the Fe_3O_4/BACell.

2.5. Synthesis of Fe_3O_4/Cell-NVP nanoparticles using the ATRP method

Firstly, in a 10 mL Schlenk flask, Cu (I) Br (28.8 mg, 0.2 mmol), PMDETA (0.042 mL, 0.2 mmol), and 5 mL DMF was added and the atmosphere was exchanged for N_2. The mixture was stirred until a homogenous blue color was seen. In a separate flask, the NVP (4 ml) was added and the Fe_3O_4/BACell nanoparticles were well dispersed via sonication in the monomer. The content of the second flask was added to the content of the schlenk flask by syringe. The schlenk flask was degassed again and the mixture was stirred in a constant temperature oil bath at 110 °C for 16 h. After the polymerization was completed, the product was isolated by an external magnetic field and then it was washed with methanol and ether to obtain the Fe_3O_4/ACell -NVP.

2.6. Loading of the DOX on the Fe_3O_4/Cell-NVP

The Doxorubicin loading was carried out on the synthesized Fe_3O_4/Cell-NVP with a certain drug concentration in water. The mixture of Fe_3O_4/ACell-NVP (2.5 mg) and the aqueous solution of the DOX (5 ml, 200ppm) was rotated at 90 rpm in the light-protected tubes at room temperature. Then, the DOX-loaded Fe_3O_4/ACell-NVP were separated by the magnetic decantation. The loading efficiency was quantified by measuring the absorbance values of the unloaded drug in the supernatant with a UV-Vis spectrophotometer at 483 nm. The loading efficiency (LE, %) was calculated according to the formula below:

$$\text{LE\%} = \frac{(\text{The total amount of drug added}) - (\text{Amount of drug in the supernatant})}{(\text{Total amount of drug added})}$$

2.7. *In vitro* drug release

Measurement of the in vitro release of the DOX from the Fe_3O_4/Cell-NVP was performed in a bicarbonate buffer (pH=5 and 7.4) at 37°C in dark using the dialysis method (cut off MW 3500). At the regular time, intervals (0.5–24 h), a 3 mL sample of the dialysate solution was withdrawn and poured back into the drug release container after measuring. The DOX concentration was determined by measuring the absorbance of the DOX in the Fe_3O_4/ACell-NVP at 483 nm by a UV-vis spectrophotometer using a calibration curve. The amount of the DOX released from the Fe_3O_4/Cell-NVP was expressed as a percentage of the total DOX and plotted as a function of time.

3. Results and discussion

3.1. Synthesis of Fe_3O_4/Cell-NVP

The proposed synthetic procedure for the preparation of the Fe_3O_4/Cell-NVP was shown in **Scheme 1**. Initially, the Fe_3O_4/BACell was synthesized through the chemical reaction of the surface of hydroxyl groups of the Fe_3O_4 nanoparticles with the methylene bromide of the BACell in the DMAc solution in presence of the pyridine. The ratio of the BACell to the Fe_3O_4 was selected in a proportion in which the free bromine groups remained on the surface of the Fe_3O_4/BACell. The Fe_3O_4/BACell with the methylene bromide on its surface acted as a macroinitiator for the ATRP of the NVP using the CuBr as a catalyst and the PMDETA as a ligand.

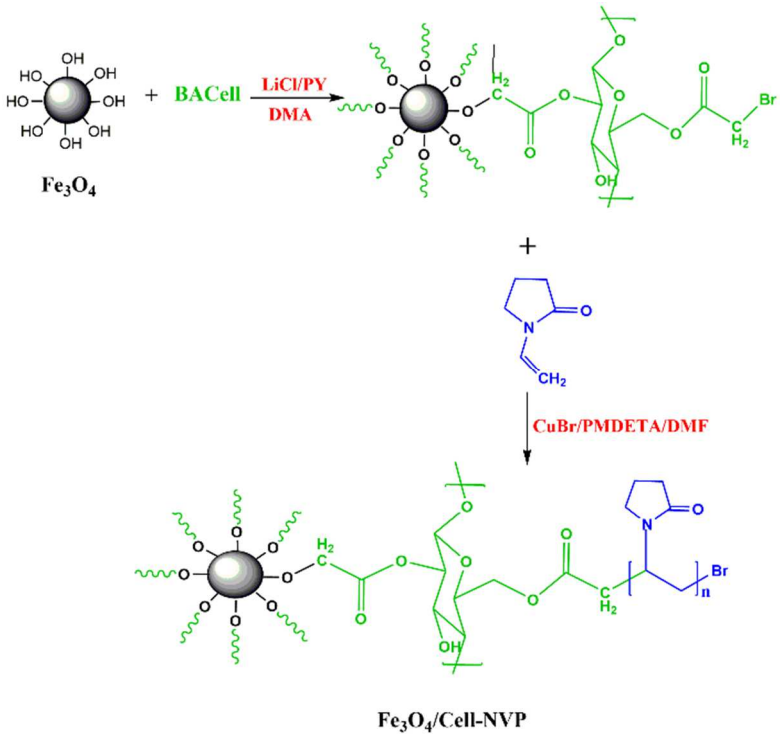

Scheme 1. Synthetic route for the preparation of Fe_3O_4/Cell-NVP.

3.2. Infrared spectroscopy (FT-IR)

The immobilization of the grafting agents on the Fe_3O_4 surface was confirmed by the FTIR. The FT-IR spectra of the pure cellulose, BACell, bare Fe_3O_4, Fe_3O_4/BACell, and Fe_3O_4/Cell-NVP are shown with descriptions in **Figure 1**. The FT-IR spectrum of the pure cellulose (**Figure 1a**) indicates the presence of the OH groups due to the bands that appear in the region between 3350-3450 cm^{-1} and they are related to the stretching vibrations of the OH ring and side-chain ($–CH_2–OH$). The band at 2900 cm^{-1} is due to the C–H stretching of the aliphatic hydrogen groups. Moreover, the ring stretching band of the glucose units appears at 1638 cm^{-1}. In addition, the bands in the region 1320–1429 cm^{-1} are due to the symmetrical deformations of the CH_2 and COH groups. The primary alcoholic CH_2OH stretching band and CH_2 twisting vibrations appear at 1058 and 1034 cm^{-1}, respectively. The weak bands at around 664 cm^{-1} are due to ring stretching and ring deformation of α-D-(1–4) and α-D-(1–6) linkages [32]. By comparing the spectrum that corresponds to the BACell (**Figure 1b**) with the pure cellulose, the O-H stretching band shifts from 3402 cm^{-1} to 3428 cm^{-1} as a result of the esterification of the O-H and the hydrogen bond dissociation. Moreover, the presence of the band at 787cm^{-1} corresponding to the carbon–bromine stretching vibration confirms the effectiveness of the bromoacetylation. The decrease in the intensity of the bands among 1050–1500 cm^{-1} which confirms the success of the reaction is due to the substitution of the hydroxyl with the acetyl bromide too. Another significant change occurs with the appearance of a sharp peak at 1754 cm^{-1} related to the formation of the ester linkage as a result of the reaction [33].

The spectra of the pure Fe_3O_4 and the Fe_3O_4/BACell can be seen in **Figure 1c** and **Figure 1d**, respectively. In **Figure 1c**, the peak at 3439 cm^{-1} is attributed to the stretching vibrations of the -OH which is assigned to the OH^- absorbed by the Fe_3O_4 nanoparticles. And the peak at 587 cm^{-1} is attributed to the Fe-O bond vibration of the Fe_3O_4 [34]. According to **Figure 1d**, the introduction of the BACell to the surface of the MNPs which is confirmed by the distinctive peaks at 3415 cm^{-1}, 1624 cm^{-1}, and 1046-1489 cm^{-1} can be related to the characteristic absorption bands of the cellulose backbone. Furthermore, the band at 1749 cm^{-1} is assigned to the ester groups of the BACell.

The FT-IR spectra of the Fe_3O_4/Cell-NVP nano-composite are shown in **Figure 1e**. The FT-IR spectra of the Fe_3O_4/Cell-NVP in comparison with the Fe_3O_4/BACell show the presence of the anchored NVP group by increasing the strength of the bands at 2920 cm^{-1} and 1650 cm^{-1} which attribute to the CH_2 and carbonyl groups of the NVP, respectively. It may also be noted that the strong absorptions due to the Fe-O bonds are evident at 587 cm^{-1} in the Fe_3O_4/BACell and the Fe_3O_4/Cell-NVP samples.

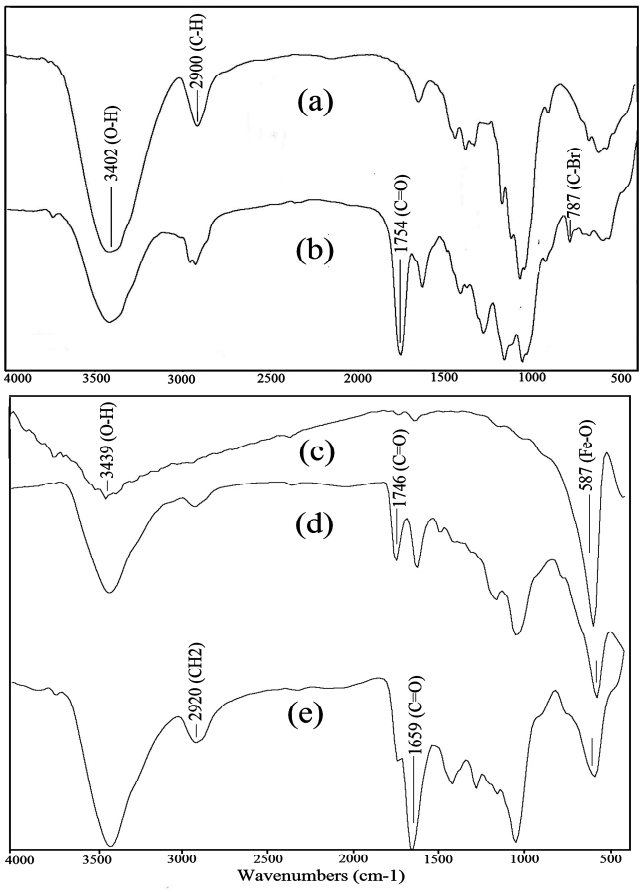

Figure 1. FT-IR spectra of (**a**) pure cellulose (**b**) BACell (**c**) pure Fe_3O_4 (**d**) Fe_3O_4/BACell (**e**) Fe_3O_4/Cell-NVP.

3.3. Scanning electron microscopy (SEM)

To evaluate the surface morphology and size distribution of the synthesized nanoparticles, we employed the SEM. The SEM images of the bare MNPs and the Fe_3O_4/Cell-NVP nanoparticles in two different magnifications are displayed in **Figure 2**. According to these images, nanoparticles at the Fe_3O_4/Cell-NVP with spherical shapes are observed, and also the size of particles mainly ranged from 80 to 200 nm. Moreover, the agglomeration is very strong in the bare Fe_3O_4 nanoparticles which is due to the Van der Waals force between the particles. The SEM images of the Fe_3O_4/Cell-NVP show that the agglomeration decreased and little aggregation is observed after a surface modification of the MNPs. Furthermore, as can be seen in **Figures 2c** and **d**, the MNPs are well distributed throughout the polymer matrix so these nanoparticles are well incorporated into a polymeric network.

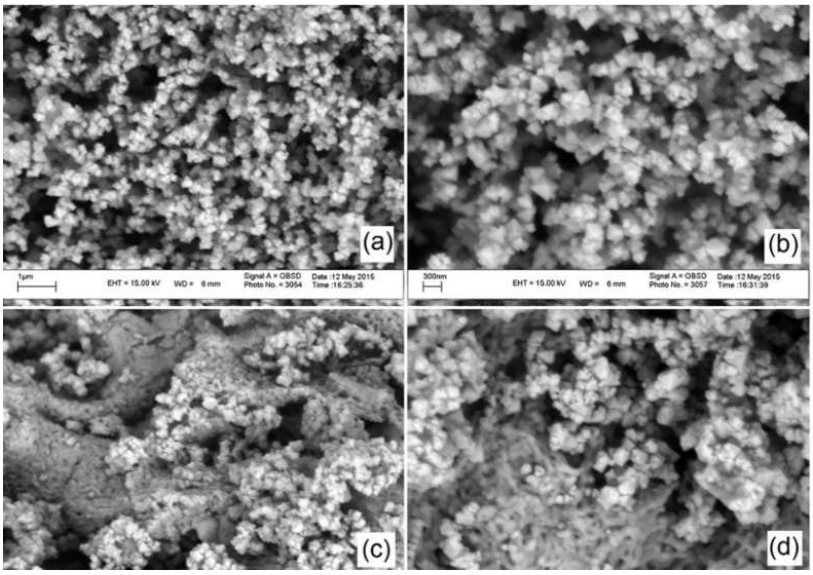

Figure 2. SEM images of (**a**), (**b**) pure Fe_3O_4 and (**c**), (**d**) Fe_3O_4/Cell-NVP

3.4. X-ray diffraction

The crystal structures of the bare Fe_3O_4 and the Fe_3O_4/Cell-NVP were also investigated. Generally, the XRD can be used to characterize the crystallinity of the nanoparticles as well as the average nanoparticle diameter [35]. From the XRD studies, as shown in **Figure 3**, the pristine MNPs exhibit shape peaks at 2θ = 30.25°, 35.61°, 43.22°, 53.59°, 57.11°, and 62.70° due to face-centered cubic lattice structures at 220, 311, 400, 331, 422, and 511, respectively [36]. The position and the relative intensities of all diffraction signals of the Fe_3O_4/Cell-NVP match well with the characteristic peaks of the magnetite crystal. The observed changes of about 2θ =10°-30° are related to the entry of the Cell-NVP polymer chains onto the surface of the nanoparticles. It means the crystalline form of the Fe_3O_4 does not change during the reaction process. The average crystallite size of the nanoparticles at the Fe_3O_4/Cell-NVP ranges from 23 to 45nm as estimated by the Scherrer equation.

$$D = \frac{k\lambda}{ß cos\theta}$$

Where D is the average crystallite size, λ the X-ray is the wavelength (0.1542 nm), ß the full-width at half-maximum (FWHM), θ the diffraction angle, and k is a constant equal to 0.89. Due to the broad diffraction pattern lines, it can be said that the particles have the size of nanometers.

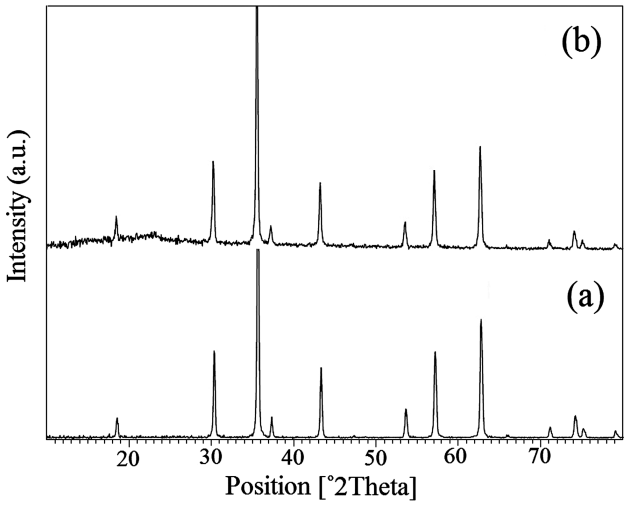

Figure 3. XRD patterns of (**a**) pure Fe_3O_4 and (**b**) Fe_3O_4/Cell-NVP

3.5. VSM measurement

Magnetic characterization of the MNPs and the Fe_3O_4/Cell-NVP is done by using the VSM and their curves are presented in **Figure 4**. According to the results in **Figure 4**, the decrease of the saturation magnetization from 66 emu/g of the bare MNP to 26 of the Fe_3O_4/Cell-NVP is attributed to the existence of the polymeric layer on the particle surface due to an effective modification reaction on the nanoparticles resulting in the decrease of the percentage of the MNP core in the modified MNPs.

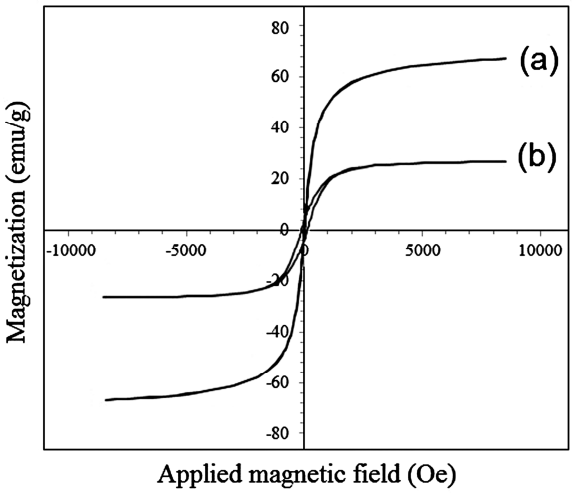

Figure 4. VSM magnetization curves of (**a**) pure Fe_3O_4 and (**b**) Fe_3O_4/Cell-NVP

3.6. Thermal gravimetric analysis (TGA)

Extracted data from TGA of the Fe_3O_4/Cell-NVP is graphically illustrated in **Figure 5**. In this graph, the degradation temperature is drawn against the amount of degradation. According to the literature [37], the TGA curve of the naked MNPs exhibits a small weight loss (about 1%) in the temperature range of 50–300 °C due to the removal of the physically and chemically adsorbed water. However, in the TGA thermogram of the Fe_3O_4/Cell-NVP a significant weight loss is observed which represents a weight fraction of the organic groups of the polymer chains. The weight loss of about 28 wt% within the temperature of 171–346°C might be due to the elimination of a side group containing the NVP repeating groups from the polymeric backbone. The next event in this process can be interpreted as the cellulose fiber decomposition from 346-650°C with 11 wt% of the weight loss. Thus, the TGA curve confirms a successful grafting onto the magnetic surface. Furthermore, the Fe_3O_4/Cell-NVP leaves 59.79% char after a complete degradation at 650 °C. This amount of char yield proves the Fe_3O_4/Cell-NVP has good thermal stability.

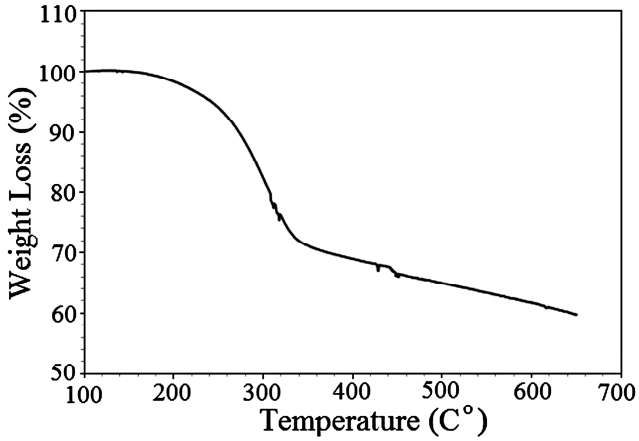

Figure 5. TGA curves for Fe_3O_4/Cell-NVP

3.7. Loading and in vitro drug release study

Drug loading capacity is an important property for an ideal drug delivery system. Loading capacity released kinetics is defined as the amount of a drug that can be mixed into the polymer network; therefore, the drug is released continuously for a longer duration after inserting it into the body. The LC % of the model drug, the DOX, is calculated in the Fe_3O_4/Cell-NVP. In this case, the LC of the MNP/mCMC is 61%. The good percentage of the LC is due to two reasons: 1. A high chain length of a polymeric shell and 2. The presence of the electronegative atoms that has a good interaction with amine, carbonyl, and carboxylic acid groups of the DOX in the polymeric layer of the nanoparticles.

It is previously reported that the pH of the tumor microenvironments has been shifted to an acidic region. Thus, the release profiles of the Fe_3O_4/Cell-NVP were investigated at a carbonate buffer with two different pH values of 5 and 7.4 to compare with each other and the results are depicted in **Figure 6**. The initial burst release can be attributed to the DOX molecules located within the concave or on the surface polymeric network. The release of the drug becomes slower after 12 hrs. and the total amount of the DOX is released within 32 hrs. The release of the DOX is quite higher at pH 5 than at pH 7.4. The fast release of the DOX in an acidic medium in comparison with a neutral medium can be attributed to the weakness of the electrostatic interactions between the drug and the carbonyl groups of the polymeric matrix as a result of the protonation of the carbonyl groups and thereby the electrostatic repulsion between the positive charges which causes the membrane to expand increases the rate of the DOX delivery. Our obtained results were compared with some similar work and the results were listed in **Table 1**. According to **Table 1**, it can be seen that the results of our synthesized nanocarrier in controlled drug release studies are satisfactory.

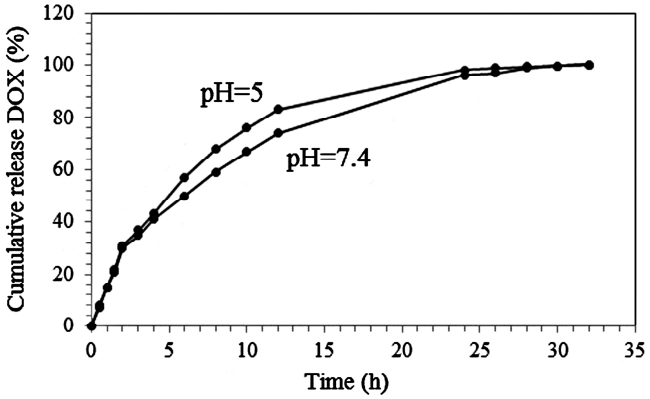

Figure 6. *In vitro* DOX release profiles from Fe_3O_4/Cell-NVP in pH 5 and pH 7.4

Table1. Comparison of the results of drug studies in some similar work.

Nanocarrier	Drug	DLE%	Drug release in pH= 5	Drug release in pH = 7.4
Fe_3O_4/Cell-NVP	DOX	61%	98% after 32h	98% after 32h
CMC-Fe_3O_4 NPs [38]	DOX	86.2%	6.30% after 144h	3.24 after 144 h
Fe_3O_4@PG/CMC-PEG [39]	DOX	65.38%	74% after 80h	34% after 80h

4. Conclusion

This work presented the surface modification of the MNP with the biocompatible and biodegradable polymeric layer via the ATRP. For this reason, firstly the magnetic nanoparticles (Fe_3O_4) were simply modified with the bromoacetylated cellulose, then polyvinyl pyrrolidone as a polymeric layer was grafted onto the surface of the MNPs via the copper-mediated ATRP of the NVP. This network was confirmed by FT-IR, SEM, VSM, TGA, and XRD. These results showed that the impact of the nanoparticles on the modified cellulose shell properties was considerable and the nanoparticles were well dispersed in the polymeric matrices; therefore, the Fe_3O_4/Cell-NVP had a superparamagnetic property. The Loading and releasing of the DOX anticancer drug on the Fe_3O_4/Cell-NVP was carried out and revealed the potential of this network for use in controlled drug delivery systems. The DOX release profiles showed a pH-dependent release pattern and also a fast release profile in an acidic medium.

Authors' contributions

All authors contributed to data analysis, drafting and revising of the paper and agreed to be responsible for all the aspects of this work.

Acknowledgments

The authors wish to acknowledge financial and spiritual support from Urmia University.

Declaration of competing interest

The authors declare no competing interest.

Funding

This paper received no external funding.

Data availability

Data will be made available on request.

References

[1] R. Mannu, V. Karthikeyan , N. Velu, Ch. Arumugam, et. al., Polyethylene Glycol Coated Magnetic Nanoparticles: Hybrid Nanofluid Formulation, Properties and Drug Delivery Prospects, Nanomaterials. 11 (2021) 440.
[2] M. Eskandari, S.H. Hosseini, M. Adeli, A. Pourjavadi, Polymer-functionalized carbon nanotubes in cancer therapy: a review, Iran Polym J. 23 (2014) 387-403.
[3] M. Mahmoudi, A. Simchi, M. Imani, P. Stroeve, A. Sohrabi, Templated growth of superparamagnetic iron oxide nanoparticles by temperature programming in the presence of poly (vinyl alcohol), Thin Solid Films. 518 (2010) 4281-4289.
[4] S. Beun, T. Glorieux, J. Devaux, J. Vreven, G. Leloup, Characterization of nanofilled compared to universal and microfilled composites, Dent Mater. 23 (2007) 51-59.
[5] M. Du, B. Guo, D. Jia, Thermal stability and flame retardant effects of halloysite nanotubes on poly(propylene), Eur Polym.J. 42 (2006) 1362-1369.
[6] A. Erten, W. rasidlo, M. Scadeng, S. Esener, R.M. Hoffman, M. Bouvet, M. Makale, Magnetic resonance and fluorescence imaging of doxorubicin-loaded nanoparticles using a novel in vivo model, Nanomedicine. 6 (2010) 797-807.
[7] F. Sharifianjazi, M. Irani, A. h. Esmaeilkhanian, L. Bazli, et.al., Polymer incorporated magnetic nanoparticles: Applications for magnetoresponsive targeted drug delivery, Mater. Sci. Eng B. 272 (2021) 115358.
[8] J.M. Shen, F.Y. Gao, T. Yin, H.X. Zhang, M. Ma, Y.J. Yang, F. Yue, cRGD-functionalized polymeric magnetic nanoparticles as a dual-drug delivery system for safe targeted cancer therapy, Pharmacol Res. 70 (2013) 102-115.
[9] H. Wang, Y. Zhao, Y. Wu, Y. Hu, K. Nan, G. Nie, Chen, H. Enhanced anti-tumor efficacy by co-delivery of doxorubicin and paclitaxel with amphiphilic methoxy PEG-PLGA copolymer nanoparticles, Biomaterials. 32 (2011) 8281-8290.
[10] E. kianfar, Magnetic Nanoparticles in Targeted Drug Delivery: A Review, J. Supercond. Nov. Magn. 34 (2021)1709–1735.
[11] M. Mohammad-Taheri, E. Vasheghani-Farahani, H. Hosseinkhani, S.A. Shojaosadati, M. Soleimani, Fabrication and characterization of a new MRI contrast agent based on a magnetic dextran–spermine nanoparticle system, Iran Polym J. 21 (2012) 239-251.
[12] Y. Choi, Electron Spin Resonance (ESR) and Microwave Absorption Studies of Superparamagnetic Iron Oxide Nanoparticles (SPIONs) for Hyperthermia Applications, J Korean Ceram Soc. 48 (2011) 577-583.
[13] E.V. Groman, J.C. Bouchard, C. P. Reinhardt, D.E.Vaccaro, Ultrasmall Mixed Ferrite Colloids as Multidimensional Magnetic Resonance Imaging, Cell Labeling, and Cell Sorting Agents**,** Bioconjug Chem. 18 (2007) 1763-1771.
[14] C. Fang, M.Q. Zhang, Multifunctional magnetic nanoparticles for medical imaging applications**,** J Mater Chem. 19 (2009) 6258-6266.
[15] H. Li, L. Qin, Y. Feng, L. Hu, C. Zhou, Preparation and characterization of highly water-soluble magnetic Fe_3O_4 nanoparticles via surface double-layered self-assembly method of sodium alpha-olefin sulfonate, J Magn Mater. 384 (2015) 213-218.
[16] J. Cai, J. Guo, M. Ji, W. Yang, C. Wang, S. Fu, Preparation and characterization of multiresponsive polymer composite microspheres with core–shell structure. Colloid Polym Sci. 285 (2007) 1607-1615.
[17] S. Wan, J. Huang, H. Yan, K. Liu, Size-controlled preparation of magnetite nanoparticles in the presence of graft copolymers. J. Mater Chem. 16 (2006) 298-303.
[18] O. Prucker, J. Ruhe, Synthesis of Poly(styrene) Monolayers Attached to High Surface Area Silica Gels through Self-Assembled Monolayers of Azo Initiators. Macromolecules. 31 (1998) 592-601.
[19] Zhao, B., Brittain, W. Polymer brushes: surface-immobilized macromolecules, J. Prog Polym Sci. 25 (2000) 677-710.
[20] Wang, H. J., Zhou, W. H., Yin, X. F., Zhuang, Z. X., Yang, H. H., Wang, X. R. Template Synthesized Molecularly Imprinted Polymer Nanotube Membranes for Chemical Separations, J Am Chem Soc. 128 (2006) 15954-15955.

[21] A. Elaissari, H. Fessi, Reactive and Highly Submicron Magnetic Latexes for Bionanotechnology Applications, Macromol Symp. 288 (2010) 115-120.
[22] S. Kayal, R.V. Ramanujan, Doxorubicin loaded PVA coated iron oxide nanoparticles for targeted drug delivery, Mater Sci Eng C. 30 (2010) 484-490.
[23] M. M. Eissa, M. M. Rahman, N. Zine, N. Jaffrezic, A. Errachid, H. Fessi, A. Elaissari, Reactive magnetic poly (divinylbenzene-co-glycidyl methacrylate) colloidal particles for specific antigen detection using microcontact printing technique, Acta Biomater. 9 (2013) 5573-5582.
[24] S. R. Ryoo, H. Jang, K. S. Kim, B. Lee, K. B. Kim, Y.K. Kim, W. S. Yeo, Y. Lee, D. E. Kim, D.H Min, Functional delivery of DNAzyme with iron oxide nanoparticles for hepatitis C virus gene knockdown. Biomaterials. 33 (2012) 2754-2761.
[25] H. Rusli, S. Gandasasmita, M. B. Amran, Cellulose acetate–silica fume membrane: characterization and application for separation of starch and maltose, Iran Polym J. 22 (2013) 335-340.
[26] S. Ehsanimehr, P. N. Moghadam,W.Dehaen,V. Shafiei- Irannejad, Synthesis of pH-sensitive nanocarriers based on polyacrylamide grafted nanocrystalline cellulose for targeted drug delivery to folate receptor in breast cancer cells, European Polymer Journal 150 (2021) 110398.
[27] S. D. Ribeiro, G. R. Filho, A. B. Meneguin, F. G. Prezotti, F. I. Boni, B. S. F. Cury, M. P. D. Gremião, Cellulose triacetate films obtained from sugarcane bagasse: Evaluation as coating and mucoadhesive material for drug delivery systems, Carbohydr. Polym. 152 (2016) 764-774.
[28] L. C. Fidale, M. Nikolajski, T. Rudolph, S. Dutz, F. H. Schacher, T. Heinze, Hybrid Fe_3O_4@amino cellulose nanoparticles in organic media – Heterogeneous ligands for atom transfer radical polymerizations, J Colloid Interface Sci. 390 (2013) 25-33.
[29] N. Mallicka, M. Asfer, M. Anwar, A. Kumar, M. Samim, S. Talegaonkar, F. Ahmad, Rhodamine-loaded, cross-linked, carboxymethyl cellulose sodium-coated super-paramagnetic iron oxide nanoparticles: Development and *in vitro* localization study for magnetic drug-targeting applications, J. Colloids Surf A. 481 (2015) 51-62.
[30] R. Elumalai, S. Patil, N. Maliyakkal, A. Rangarajan, P. Kondaiah, A. M. Raichur, Protamine-carboxymethyl cellulose magnetic nanocapsules for enhanced delivery of anticancer drugs against drug resistant cancers, Nanomedicine. 11 (2015) 969-981.
[31] M. C. I. M. Amin, N. Ahmad, N. Halib, I. Ahmad, Synthesis and characterization of thermo-and pH-responsive bacterial cellulose/acrylic acid hydrogels for drug delivery, Carbohydr. Polym. 88 (2012) 465– 473.
[32] Y. MinKim, Y. SukLee, T. Kim, K. Yang, K. Nam, D. Choe, Y. HoonRoh, Cationic cellulose nanocrystals complexed with polymeric siRNA for efficient anticancer drug delivery, Carbohydr. Polym. 247 (2020) 116684.
[33] J. Song, N. L. Birbach,J. P. Hinestroza,Deposition of silver nanoparticles on cellulosic fibers via stabilization of carboxymethyl groups, Cellulose. 19 (2012) 411–424.
[34] S. Ehsanimehr, P. N. Moghadam,W.Dehaen, V. Shafiei- Irannejad, PEI grafted Fe_3O_4@SiO_2@SBA-15 labeled FA as a pH-sensitive mesoporous magnetic and biocompatible nanocarrier for targeted delivery of doxorubicin to MCF-7 cell line, Colloids and Surfaces A: Physicochemical and Engineering Aspects 615 (2021) 126302.
[35] O. Ayala-Valenzuela, J. Matutes-Aquino, R. Betancourt-Galindo, L.A. Garcia-Cerda, F. O. Rodriíguez, P. C. Fannin, A. T. Giannitsis, Characterization of soft ferromagnetic materials by inductance spectroscopy and magnetoimpedance, J Magn Mater. 294 (2005) 239-244.
[36] Z. Shokri, B. Zeynizadeh, S.A. Hosseini, One-pot reductive-acetylation of nitroarenes with NaBH4 catalyzed by separable core-shell Fe_3O_4@Cu (OH) x nanoparticles, J. Colloid Interf. Sci. 485(2017) 99.
[37] F. Galeotti, F. Bertini, G. Scavia, A. Bolognesi, A controlled approach to iron oxide nanoparticles functionalization for magnetic polymer brushes, J Colloid Interface Sci. 360 (2011) 540-547.
[38] T. Gürkan Polat, S.Demirel Topel, pH-responsive carboxymethyl cellulose conjugated superparamagnetic iron oxide nanocarriers, J Sci Perspectives.3 (2019) 99-110.
[39] N. Zohreh, N. Karimi,S. H. Hosseini,C. Istrate ,C. Busuioc, Fabrication of a magnetic nanocarrier for doxorubicin delivery based on hyperbranched polyglycerol and carboxymethyl cellulose: An investigation on the effect of borax cross-linker on pH-sensitivity.Int. J. Biol. Macromol.203 (2022) 80-92.